CrossMark

Cu–Sn and Ni–Sn transient liquid phase bonding for die-attach technology applications in high-temperature power electronics packaging

Byung-Suk Lee[1,2] · Soong-Keun Hyun[2] · Jeong-Won Yoon[1,3]

Abstract Power electronics modules in electric vehicles and hybrid electric vehicles, particularly those containing next-generation power semiconductor devices such as silicon carbide and gallium nitride are operated at high temperatures exceeding 200 °C. Consequently, the reliability requirements for such modules have become highly stringent and new packaging materials and technologies are required to meet the demands of power electronic modules. Some good candidates for high temperature applications include high-temperature solders such as Au–20Sn, Ag or Cu sinter pastes, and transient liquid phase (TLP) bonding materials. In particular, the TLP bonding technology is suitable for use in high temperature environments owing to its low cost and simplicity of the bonding process. In this study, the feasibility of Cu–Sn and Ni–Sn TLP bonding technologies as die-attach methods for power electronics packaging applications is examined. The results of the study indicate that the Cu–Sn and Ni–Sn TLP bonding processes transform the joints fully into Cu_6Sn_5/Cu_3Sn and Ni_3Sn_4 intermetallic compounds (IMCs), respectively. Further, the mechanical strength and reliability of the two TLP bonding joints are reduced owing to the formation of brittle IMCs.

✉ Jeong-Won Yoon
  jwyoon@kitech.re.kr

1   Welding and Joining R&D Group, Korea Institute
    of Industrial Technology (KITECH), 156 Gaetbeol-ro,
    Yeonsu-gu, Incheon 21999, South Korea

2   Department of Metallurgical Engineering, Inha University,
    Incheon 22212, South Korea

3   Critical Materials and Semiconductor Packaging
    Engineering, University of Science and Technology (UST),
    217 Gajeong-ro, Yuseong-gu, Daejeon 34113, South Korea

1 Introduction

In recent years, various global environmental pollution control policies such as the restriction of hazardous substances directive and the end of life vehicle regulation have been enacted. Consequently, eco-friendly vehicles such as hybrid electric vehicles and electric vehicles have come into focus. In such eco-friendly vehicles, power modules convert electrical energy into mechanical energy and power electronics packaging is a key class of technologies required for fabricating such power modules [1]. Moreover, power electronics packaging technologies are required for ensuring efficient power conversion with the semiconductor devices in the power modules. Increases in the operating temperatures and current densities of advanced power devices enhance the complexities involved in meeting the quality requirements of power electronic modules [2]. So far, Pb-containing solder alloys have been widely used as die-attach materials between the chips and substrate in power electronics packaging [3]. However, a number of studies have focused on replacing the Pb-bearing alloys, because they are toxic, not reliable enough, and are unable to withstand the high operating temperatures required in specific applications. In the current power electronics industry, many manufacturers aim to increase the chip junction temperature to 200 °C and even beyond. Generally, Pb-free solder alloys are difficult to use over long durations at high temperatures, owing to relatively poor thermal characteristics such as low melting point and thermal fatigue [3–6]. In addition, Si is likely to be replaced with wide band gap semiconductors such as silicon carbide and gallium nitride in devices designed for high-temperature operations, owing to the excellent thermal characteristics of the latter. Thus, new interconnect materials and technologies are required before high-temperature devices and

🙛 Springer

circuits can be scaled-up and reliably incorporated into power electronics systems. Examples of such technologies include soldering with high-melting temperature solders, sintering with Ag or Cu metal powders, and diffusion soldering or transient liquid phase (TLP) bonding. Au–Sn solder [7–10] and Ag paste [11–13] are available as suitable alternative bonding materials. However, they are relatively expensive owing to the use of noble metals such as Au and Ag. In contrast, the TLP bonding technology utilizes cheap metals such as Cu, Ni, and Sn. This process is also similar to the soldering process and is reliable when subjected to high temperatures over long durations. TLP bonding is a die-attach technology wherein an intermetallic compound (IMC) is formed via a diffusion reaction by incorporating a low melting point metal between metals with high melting points. The resulting IMC plays the role of an attach material for the TLP bonded joints and is suitable for high-temperature operation, owing to the increased re-melting point. The joints bonded using typical Sn-based solders do not melt unless the assembly is heated to the melting point of the IMC phases (i.e., 415 °C for Cu_6Sn_5, 676 °C for Cu_3Sn, and 794 °C for Ni_3Sn_4). Two metals that are able to form IMCs at low temperatures can be used as materials for TLP bonding [14–16]. Recently, the TLP bonding technology has gained significant attention owing to such advantages in power electronics packaging.

In the current study, Cu–Sn and Ni–Sn TLP bonding technologies have been investigated as die-attach methods for power electronics packaging. We first evaluated the interfacial reactions and transformation of the solder to the IMC phase under various TLP bonding conditions. In order to determine the effect of interfacial reactions and reaction products on the mechanical properties of the TLP bonded joints, lap shear tests were conducted. Further, the relationship between the mechanical properties of the TLP bonded joints and interfacial reactions is discussed.

2 Experimental procedure

Two TLP bonding specimens made of Cu/Sn/Cu and Ni/Sn/Ni were used in this study. Substrates consisting of 200 μm-thick Cu coupons were used for the two TLP bonding tests. To form the Cu–Sn TLP bonding, a 7 μm thick Sn layer was plated on the Cu substrate, whereas in the case of Ni–Sn TLP bonding, Ni(P) was plated electrolessly. The electroless Ni(P) layer was about 5 μm thick and contained approximately 15 at.% P. Subsequently, a 7 μm thick Sn layer was plated over the Ni(P) layer. The bonding processes for the two materials were performed under identical conditions. The Sn-coated substrates were bonded to other Sn-coated substrates using flux in a vacuum reflow machine (SRO-704, ATV Technologie GmbH, Germany). Figure 1a, b show schematic illustrations of the Cu/Sn/Cu and Ni/Sn/Ni samples. During the bonding process, the samples were exposed to a N_2 atmosphere in the chamber of the vacuum reflow machine. The maximum bonding temperature was 300 °C and five bonding durations, namely 4, 30 min, 1, 2, and 3 h were examined. After the bonding process, the samples were cooled to room temperature and their cross-sections were examined. To prepare the samples for cross-sectional analysis, common metallographic procedures
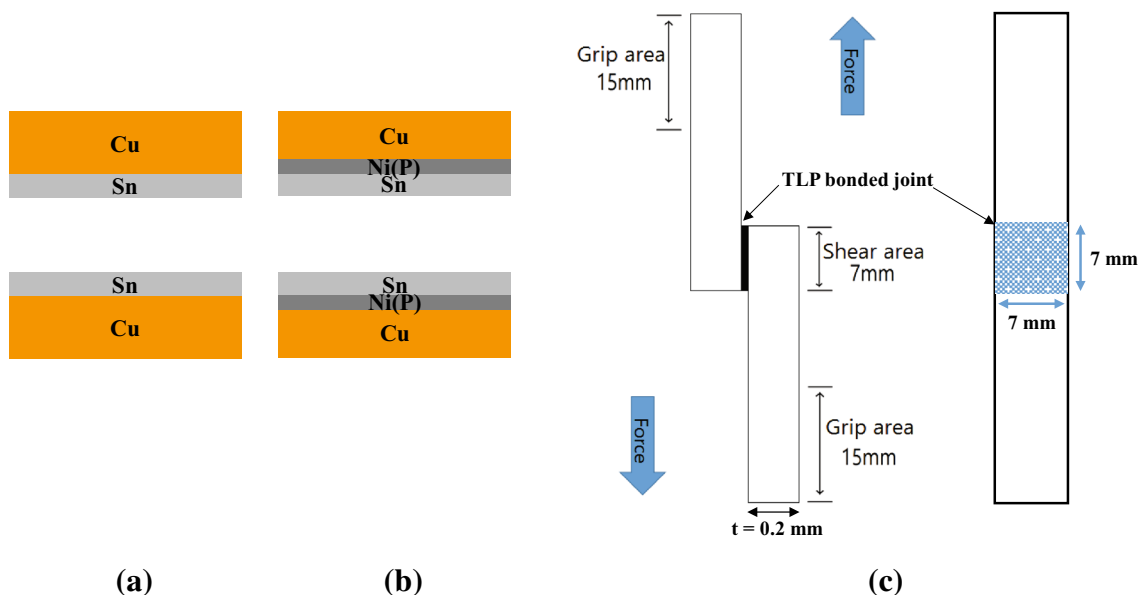
Fig. 1 Schematic diagrams of **a** Cu/Sn/Cu joint, **b** Ni/Sn/Ni joint, and **c** lap shear test samples and lap shear testing methodology

including grinding and polishing were used and an etchant consisting of 95% C_2H_5OH-4% HNO_3-1% HCl was used to reveal the microstructure in the cross-section of the samples. The microstructures and chemical compositions were determined using a scanning electron microscope (SEM, INSPECT F, FEI, USA) equipped with an energy dispersive X-ray spectroscope (EDX). In order to determine the effect of interfacial reactions and IMC formation during TLP bonding on the mechanical properties of the TLP bonded joints, lap shear tests were conducted using a global lap shear tester (LR30K-plus, LLOYD instruments LTD). Figure 1c shows a schematic diagram of the lap shear testing methodology and the samples used for these tests. The lap shear test samples had a grip area of 15×7 mm, shear area of 7×7 mm, and thickness of 0.2 mm. The tests were performed according to the ASTM D1002 standard [17] with a speed of 1.3 mm/min. A total of seven lap shear samples was tested under each condition and the average values are reported. After the lap shear tests, the fracture surfaces were investigated thoroughly using SEM and EDX.

3 Results and discussion

Figure 2 shows cross-sectional SEM images of the Cu/Sn/Cu TLP joints subjected to bonding at 300 °C for various durations of time. The Cu–Sn TLP bonded joints were formed by melting Sn between two Cu layers. During the reflow process, the Sn solder was in the molten state and typical scallop-type Cu_6Sn_5 IMCs were formed at both interfaces. A bond line thickness (BLT) of approximately 15 μm was achieved after a bonding time of 4 min (Fig. 2a). After bonding for 30 min, Cu_3Sn IMCs were formed at both the interfaces between the Cu_6Sn_5 layer and Cu substrate, as shown in Fig. 2b. Therefore, Cu_6Sn_5 and Cu_3Sn are the main reaction products in the Cu–Sn system. The size of the Cu_6Sn_5 IMCs increased with increase in the bonding time. Till a bonding time of 30 min, a Sn layer was present between the two Cu_6Sn_5 IMC layers, whereas after a bonding time of 1 h, large Cu_6Sn_5 IMCs were formed in

the TLP bonded joint, and both the Cu substrates were connected via the Cu_6Sn_5 IMCs, as shown in Fig. 2c. However, Sn still remained in the TLP bonded joint. After a bonding time of 2 h, the TLP bonded joints were completely transformed into the Cu_6Sn_5 and Cu_3Sn IMCs. Further, Sn was completely consumed and was no longer present in the joint (Fig. 2d). After a bonding time of 3 h, the thickness of the Cu_3Sn IMC layer between the Cu layer and Cu_6Sn_5 IMC increased (Fig. 2e). On the other hand, between 2 and 3 h, Cu_6Sn_5 was transformed into the Cu_3Sn IMC, owing to the depletion of Sn and further diffusion of Cu atoms. These processes resulted in the formation of relatively thick Cu_3Sn IMCs. After a reaction time of 3 h, the thicknesses of the reaction products, Cu_6Sn_5, and Cu_3Sn were 7.5 and 7.5 μm, respectively. Overall, the BLTs were distributed uniformly, with the thickness ranging from 15 to 16.8 μm during TLP bonding. Thus, we successfully fabricated Cu–Sn TLP bonded joints composed of Cu_6Sn_5 and Cu_3Sn IMCs in this study.

Figure 3 shows cross-sectional SEM images of the Ni/Sn/Ni TLP joints subjected to bonding at 300 °C for various durations. TLP bonding for 4 min yielded typical needle-type Ni_3Sn_4 IMCs at both the interfaces as shown in Fig. 3a. In addition, Ni_3P layers were formed at the two interfaces between the Ni_3Sn_4 IMC and electroless Ni(P) layer. This Ni_3P layer contained about 25 at.% P, as determined from the EDX analysis. The formation of the Ni_3P layer in the Sn-based solder/Ni(P) system is well-known from previous reports [18, 19]. After 30 min, many needle-type Ni_3Sn_4 IMCs were formed at both the interfaces. In addition, the Ni_3P layer grew in thickness with increase in the bonding time (Fig. 3b). While after a bonding time of 1 h, the bonded joint was mostly transformed into Ni_3Sn_4 IMCs, we also observed a small amount of remaining Sn in the center of the TLP bonded joint, as shown in Fig. 3c. After a reaction time of 2 h, the TLP bonded joints were completely transformed into the Ni_3Sn_4 IMCs, as shown in Fig. 3d. In addition, the Ni(P) layer was also completely converted into the Ni_3P layer, which contained a number of voids owing to the transformation from amorphous


(a) 4 min	**(b)** 30 min	**(c)** 1 h	**(d)** 2 h	**(e)** 3 h
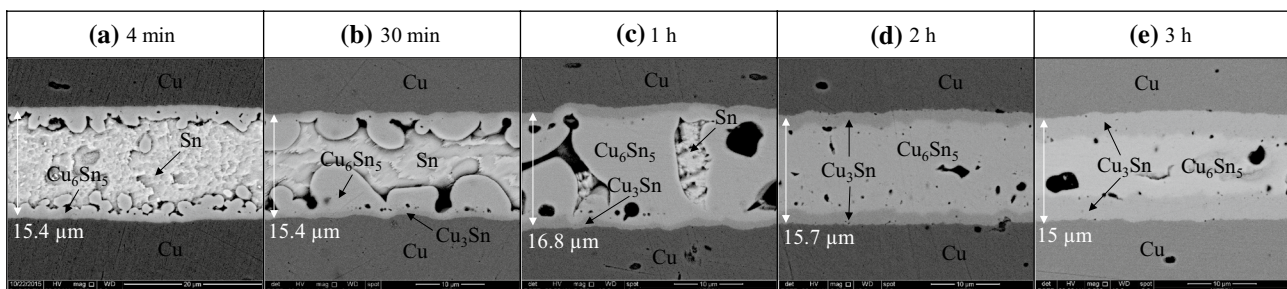
Fig. 2 Cross-sectional SEM micrographs of Cu/Sn/Cu TLP bonded interfaces subjected to bonding at 300 °C for various durations: **a** 4 min, **b** 30 min, **c** 1 h, **d** 2 h, and **e** 3 h
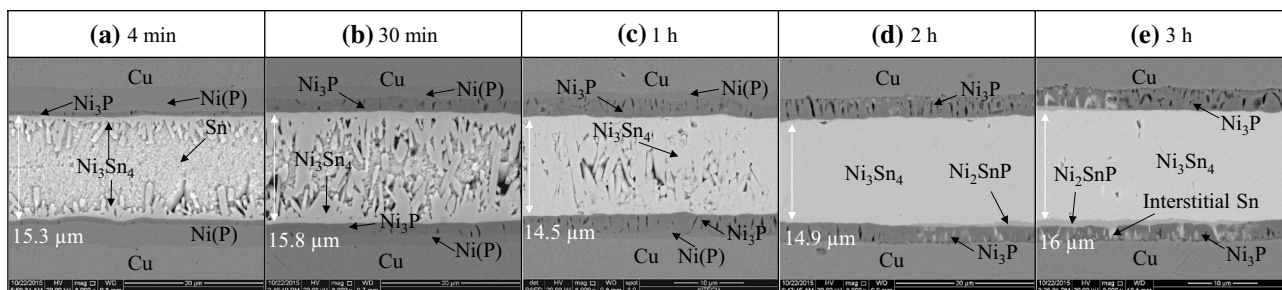
Fig. 3 Cross-sectional SEM micrographs of the Ni/Sn/Ni TLP bonded interfaces bonded at 300 °C for various durations: **a** 4 min, **b** 30 min, **c** 1 h, **d** 2 h, and **e** 3 h

Ni(P) to the crystalline Ni_3P phase [20]. Another ternary Ni_2SnP layer was also observed between the Ni_3Sn_4 IMC and Ni_3P layer. Similar results have been reported in previous papers [20, 21]. After TLP bonding for 3 h, no significant changes in microstructure were observed, because Sn was completely consumed after 2 h (Fig. 3e). There was only a slight increase in the thickness of the ternary Ni_2SnP layer and more interstitial Sn was observed in the Ni_3P layer. Similar to the Cu–Sn TLP bonding shown in Fig. 2, the BLTs were uniformly distributed with the thickness ranging from 14.5 to 16 μm during Ni–Sn TLP bonding. In this study, BLTs of approximately 15 μm were achieved for both Cu–Sn and Ni–Sn TLP bonding. We used bonding temperature of 300 °C and bonding time up to 3 h without bonding pressure in our TLP bonding process. Therefore, we obtained a relative thick bond line thickness of about 15 μm. We can reduce BLTs by using moderate bonding pressure and thinner Sn layer between Cu or Ni metal layer. In the TLP bonding process, the bonding thickness is an important issue in the successful TLP bonding and formation of a robust joint. In addition, the process time is strongly related to the TLP bonding thickness. Therefore, we can control the interfacial reactions, interfacial microstructure, and phase formation by modifications of bonding parameters such as pressure, temperature, and time.

The interfacial microstructure of the bonded joints is closely related to the mechanical strength and reliability of the bonded joints, in general [22–25]. Therefore, we performed lap shear tests to evaluate the effect of interfacial reactions and IMC formation on the mechanical properties of the TLP bonded Cu/Sn/Cu and Ni/Sn/Ni joints. Figure 4 shows the lap shear strengths of the two TLP bonded joints at various bonding durations. In the case of the Cu/Sn/Cu joints, the shear strength tended to decrease abruptly after bonding for 30 min. The average shear strength of the Cu/Sn/Cu joints after bonding for 4 min was about 7 MPa, whereas this value decreased to 2 MPa after bonding for 30 min. Further increased in the bonding time from 30 min to 3 h did not lead to changes in the shear strength and a constant value of about 2 MPa
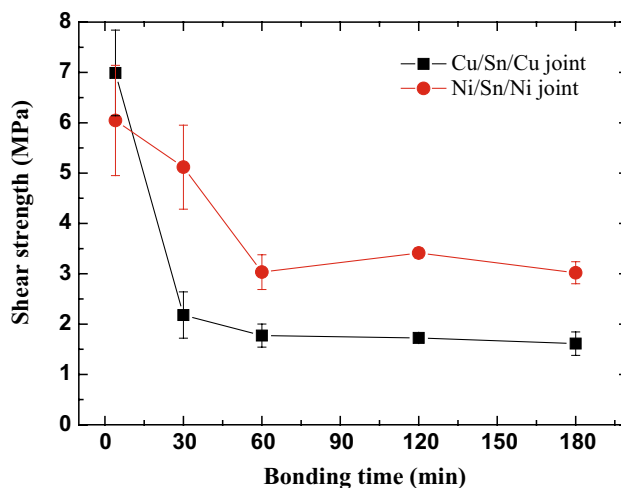
Fig. 4 Shear strength variation of the Cu/Sn/Cu and Ni/Sn/Ni TLP bonded joints as a function of bonding time. The *error bars* are determined from the maximum and minimum strength values obtained from seven test samples

was observed. On the other hand, in the case of the Ni/Sn/Ni joints, the shear strength tended to decrease with increase in the bonding time up to 1 h, as shown in Fig. 4. The average shear strength of the Ni/Sn/Ni joints after bonding for 4 min was about 6 MPa, which decreased to 5 and 3 MPa after bonding for 30 min and 1 h, respectively. After a bonding time of 1 h, constant shear strength values were obtained. The shear strengths of the Cu/Sn/Cu and Ni/Sn/Ni joints decreased significantly after bonding for 30 min and 1 h, respectively. However, large deviations in these values were observed. As shown in Figs. 2 and 3, the TLP bonded joints for the two types of samples were transformed into the IMC phase after a bonding time of 2 h. In this case, the Ni/Sn/Ni joints had a slightly higher strength (3 MPa) compared to the Cu/Sn/Cu joints (2 MPa), owing to the formation of different IMCs in Cu–Sn and Ni–Sn [26]. As whole, low shear strength values of 2–7 MPa are measured in this study. According to a literature [27], die shear strength values of

approximately 11 and 9–16 MPa are reported for Au–Sn and Cu–Sn TLP bonded joints, respectively. Although the exact reason for the difference in shear strength is not clear at this point, it is presumably due to the discrepancy of small and large bonding area, used metallizations, shear test methods such as lap shear and die shear, and existence of defects as a void.

To confirm the variations in the lap shear strength, the fracture surfaces after lap shear testing were thoroughly examined by SEM. Figure 5 shows the cross-sectional SEM micrographs of the fractured Cu/Sn/Cu joints subjected to bonding for various durations of time. It may be observed that fracture occurred in the bulk Sn solder after bonding for 4 min. The remaining Sn is indicated with red lines in Fig. 5a. However, after bonding for 30 min, IMC fracture occurred. Although complete transformation to the IMC did not occur and Sn remained after a bonding duration of 30 min (Fig. 2b), fracture mainly occurred along the Cu_6Sn_5 IMC interfaces (Fig. 5b). This caused the abrupt decrease in the lap shear strength after 30 min of bonding in the case of the Cu/Sn/Cu joints, as shown in Fig. 4. After prolonged bonding up to 3 h, brittle IMC fractures were also observed.

Figure 6 shows the cross-sectional SEM micrographs of the fractured Ni/Sn/Ni joints at various bonding durations. When the Ni/Sn/Ni TLP samples were bonded at 300 °C, fracture occurred in the bulk Sn solder up to a bonding time

of 30 min, whereas fracture was observed at the IMC interface after bonding for 1 h. These results are consistent with the shear strength results shown in Fig. 4.
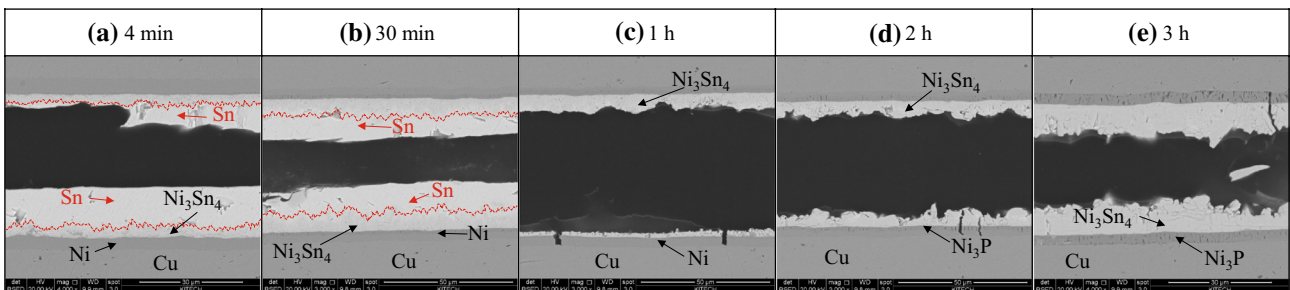
A schematic illustration of the fracture sites in the two TLP bonded joints is shown in Fig. 7. This diagram is constructed based on the results shown in Figs. 2, 3, 4, 5 and 6. We overlapped the fracture sites observed in the cross-sectional SEM micrographs, and the Sn solder and IMC fractures are indicated using red and blue lines, respectively. Fracture mostly occurred along the center lines regardless of IMC growth in the two TLP bonded joints. During the initial bonding stages, remaining Sn was observed and small IMCs were formed at both the interfaces, resulting in high shear strength. On the other hand, complete transformation to Cu–Sn or Ni–Sn IMCs reduced the shear strength of the TLP bonded joints. Although the TLP bonded joints were able to withstand temperatures above the bonding temperature, once they were completely transformed into the IMC phases, the TLP joint became brittle.

4 Conclusions

We compared the interfacial reaction behavior and mechanical reliability of the Cu–Sn and Ni–Sn TLP bonded joints. The relationships between the bonding conditions, interfacial microstructure, and mechanical
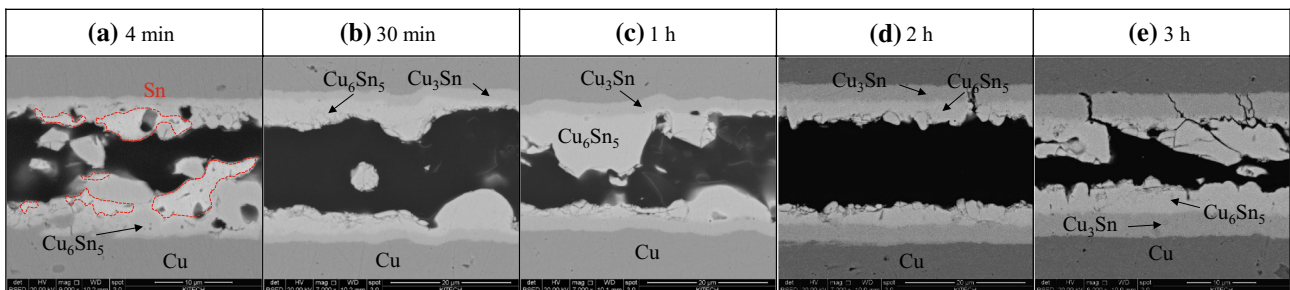
Fig. 5 Cross-sectional SEM micrographs of the fractured Cu/Sn/Cu TLP bonded joints as a function of bonding time: **a** 4 min, **b** 30 min, **c** 1 h, **d** 2 h, and **e** 3 h

Fig. 6 Cross-sectional SEM micrographs of the fractured Ni/Sn/Ni TLP bonded joints as a function of bonding time: **a** 4 min, **b** 30 min, **c** 1 h, **d** 2 h, and **e** 3 h
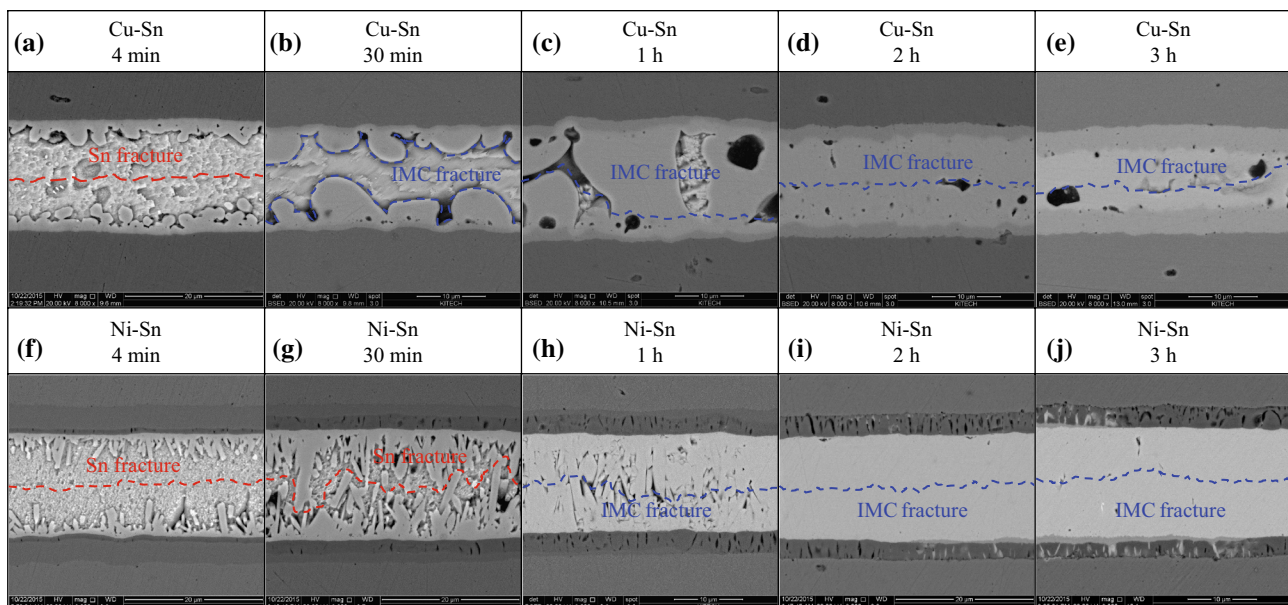
Fig. 7 Schematic diagrams of the fracture sites at the Cu/Sn/Cu and Ni/Sn/Ni TLP bonded joints; **a–e** Cu/Sn/Cu TLP bonded joints and **f–j** Ni/Sn/Ni TLP bonded joints

strength are investigated in this paper. In the case of the Cu–Sn TLP bonding, Cu_6Sn_5 IMC grew in thickness by consuming the Sn layer between 4 min and 1 h of bonding. The interfaces of the Cu–Sn TLP bonded joints were completely transformed to the Cu_6Sn_5 and Cu_3Sn IMCs after 2 h. In the case of Ni–Sn TLP bonding, only Ni_3Sn_4 IMCs were formed at the interface. In addition, Ni_2SnP, Ni_3P, and interstitial Sn were also observed in the TLP bonded joint after 2 h. The shear strength of the two TLP bonded joints significantly decreased during the initial stages of bonding, resulting in transition from ductile to brittle fracture. This is attributed to the formation of the IMC layers and weak interfaces. The shear strength of the Cu–Sn TLP bonded joints were more rapidly reduced compared to the Ni–Sn TLP bonded joints. More reliability studies are required before the TLP bonded joints can be reliably incorporated into power electronics systems.

References

1. Y. Wang, S. Jones, A. Dai, G. Liu, Microelectron. Reliab. **54**, 1911–1915 (2014)
2. A. Ibrahim, J.P. Ousten, R. Lallemand, Z. Khatir, Microelectron. Reliab. **58**, 204–210 (2016)
3. F.P. McCluskey, M. Dash, Z. Wang, D. Huff, Microelectron. Reliab. **46**, 1910–1914 (2006)
4. Z. Liang, IEEE Power Electronics Society, in *Proceedings of International Symposium on Power Semiconductor Devices and ICs (ISPSD)* (2012), pp. 325–331
5. C. Buttay, D. Planson, B. Allard, D. Bergogne, P. Bevilacqua, C. Joubert, M. Lazar, C. Martin, H. Morel, D. Tournier, C. Raynaud, Mater. Sci. Eng. B **176**, 283–288 (2011)
6. H. Ji, M. Li, S. Ma, M. Li, Mater. Des. **108**, 590–596 (2016)
7. S. Anhock, H. Oppermann, C. Kallmayer, R. Aschenbrenner, L. Thomas, H. Reichl, in *Proceedings of IEEE Electronics Manufacturing Technology Symposium* (1998), pp. 156–165
8. Y.C. Liu, J.W.R. Teo, S.K. Tung, K.H. Lam, J. Alloys Compd. **448**, 340–343 (2008)
9. J.W. Yoon, H.S. Chun, S.B. Jung, J. Alloys Compd. **469**, 108–115 (2009)
10. G.S. Matijasevic, C.C. Lee, C.Y. Wang, Thin Solid Films **223**, 276–287 (1993)
11. C. Gobl, J. Faltenbacher, in *Proceedings of the 6th International Conference on IEEE Integrated Power Electronics Systems (CIPS)* (2010), pp. 1–5
12. T.G. Lei, J.N. Calata, G.Q.L.X. Chen, S. Luo, IEEE Trans. Comp. Pack. Technol. **33**, 98–104 (2010)
13. M. Knoerr, A. Schletz, in *Proceedings of the 6th International Conference on IEEE Integrated Power Electronics Systems (CIPS)* (2010), pp. 1–6
14. S.W. Yoon, M.D. Glover, K. Shiozaki, IEEE Trans. Power Electron **28**, 2448–2456 (2013)
15. T.A. Tollefsen, A. Larsson, O.M. Lovvik, K.E. Aasmundtveit, IEEE Trans. Compon. Pack. Manuf. Technol. **3**, 904–914 (2013)
16. S.W. Yoon, K. Shiozaki, S. Yasuda, M.D. Glover, in *Proceedings of the IEEE Applied Power Electronics Conference and Exposition (APEC)* (2012), pp. 478–482
17. ASTM D1002-10, Standard test method for apparent shear strength of single-lap-joint adhesively bonded metal specimens by tension loading (Metal-to-Metal), ASTM International, West Conshohocken, PA (2010)
18. J.W. Yoon, S.B. Jung, J. Alloys Compd. **376**, 105–110 (2004)
19. K. Zeng, K.N. Tu, Mater. Sci. Eng. R **38**, 55–105 (2002)
20. H.S. Chun, J.W. Yoon, S.B. Jung, J. Alloys Compd. **439**, 91–96 (2007)

21. H.B. Kang, J.H. Bae, J.W. Yoon, S.B. Jung, J.W. Park, C.W. Yang, Scripta Mater. **63**, 1108–1111 (2010)
22. J.W. Yoon, S.W. Kim, S.B. Jung, Mater. Trans. **45**, 727–733 (2004)
23. Y.C. Chan, A.C.K. So, J.K.L. Lai, Mater. Sci. Eng. B **55**, 5–13 (1998)
24. P.L. Tu, Y.C. Chan, K.C. Hung, J.K.L. Lai, Scripta Mater. **44**, 317–323 (2001)
25. R.E. Pratt, E.I. Stromswold, D.J. Quesnel, IEEE Trans. Compon. Pack. Manuf. Technol **19**, 134–141 (1996)
26. C.C. Lee, P.J. Wang, J.S. Kim, in Proceedings of the 57th International Conference on Electronic Components and Technology Conference (ECTC) (2007), pp. 648–652
27. N. Hoivik, H. Liu, K. Wang, G. Salomonsen, K. Aasmundtveit, in Advanced Materials and Technologies for Micro/Nano-Devices, Sensors and Actuators, ed. by E. Gusev, E. Garfunkel, A. Dideikin (Springer, Dordrecht, 2010), p. 189